RESEARCH ARTICLE

Impaired HLA Class I Antigen Processing and Presentation as a Mechanism of Acquired Resistance to Immune Checkpoint Inhibitors in Lung Cancer

Scott Gettinger[1,2], Jungmin Choi[3], Katherine Hastings[2], Anna Truini[2], Ila Datar[4], Ryan Sowell[5], Anna Wurtz[2], Weilai Dong[3], Guoping Cai[4], Mary Ann Melnick[2], Victor Y. Du[5], Joseph Schlessinger[2,6], Sarah B. Goldberg[1,2], Anne Chiang[1,2], Miguel F. Sanmamed[5], Ignacio Melero[7,8], Jackeline Agorreta[7,8], Luis M. Montuenga[7,8], Richard Lifton[3], Soldano Ferrone[9], Paula Kavathas[2,5,10], David L. Rimm[2,4], Susan M. Kaech[2,5], Kurt Schalper[1,2,4], Roy S. Herbst[1,2,6], and Katerina Politi[1,2,4]

ABSTRACT

Mechanisms of acquired resistance to immune checkpoint inhibitors (ICI) are poorly understood. We leveraged a collection of 14 ICI-resistant lung cancer samples to investigate whether alterations in genes encoding HLA Class I antigen processing and presentation machinery (APM) components or interferon signaling play a role in acquired resistance to PD-1 or PD-L1 antagonistic antibodies. Recurrent mutations or copy-number changes were not detected in our cohort. In one case, we found acquired homozygous loss of *B2M* that caused lack of cell-surface HLA Class I expression in the tumor and a matched patient-derived xenograft (PDX). Downregulation of B2M was also found in two additional PDXs established from ICI-resistant tumors. CRISPR-mediated knockout of *B2m* in an immunocompetent lung cancer mouse model conferred resistance to PD-1 blockade *in vivo*, proving its role in resistance to ICIs. These results indicate that HLA Class I APM disruption can mediate escape from ICIs in lung cancer.

SIGNIFICANCE: As programmed death 1 axis inhibitors are becoming more established in standard treatment algorithms for diverse malignancies, acquired resistance to these therapies is increasingly being encountered. Here, we found that defective antigen processing and presentation can serve as a mechanism of such resistance in lung cancer. *Cancer Discov; 7(12); 1420–35. ©2017 AACR.*

[1]Department of Medicine (Section of Medical Oncology), Yale University School of Medicine, New Haven, Connecticut. [2]Yale Cancer Center, Yale University School of Medicine, New Haven, Connecticut. [3]Department of Genetics, Yale University School of Medicine, New Haven, Connecticut. [4]Department of Pathology, Yale University School of Medicine, New Haven, Connecticut. [5]Department of Immunobiology, Yale University School of Medicine, New Haven, Connecticut. [6]Department of Pharmacology, Yale University School of Medicine, New Haven, Connecticut. [7]CIMA and Clinica Universidad de Navarra, Pamplona, Spain. [8]Centro de Investigación Biomédica en red de Oncología CIBERONC, Madrid, Spain. [9]Department of Surgery, Massachusetts General Hospital, Harvard Medical School, Boston, Massachusetts. [10]Department of Laboratory Medicine, Yale University School of Medicine, New Haven, Connecticut.

Note: Supplementary data for this article are available at Cancer Discovery Online (http://cancerdiscovery.aacrjournals.org/).

S. Gettinger, J. Choi, K. Hastings, A. Truini, and I. Datar contributed equally to this article.

Current address for R. Lifton: The Rockefeller University, New York, New York.

Corresponding Authors: Katerina Politi, Yale University School of Medicine, 333 Cedar Street, SHM-I 234D, New Haven, CT 06510. Phone: 203-737-5921, Fax: 203-785-7531; E-mail: katerina.politi@yale.edu; and Scott Gettinger, Department of Internal Medicine (Section of Medical Oncology), Yale Cancer Center, Yale University School of Medicine, New Haven, CT 06520. Phone: 203-737-6980; Fax: 203-785-3788; E-mail: scott.gettinger@yale.edu

doi: 10.1158/2159-8290.CD-17-0593

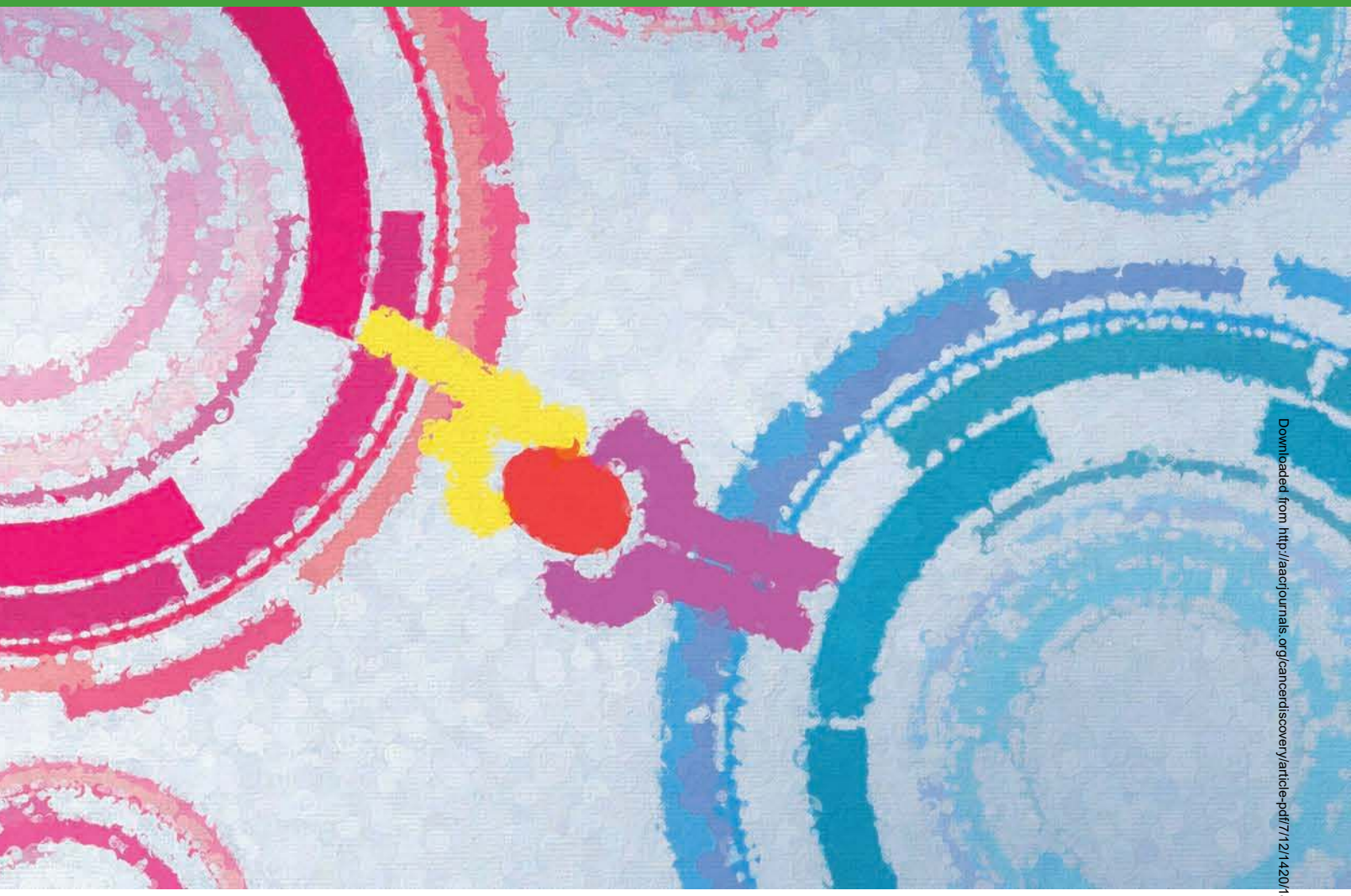

INTRODUCTION

Recent regulatory agency approvals of immune checkpoint inhibitors (ICI), including programmed death 1 (PD-1), programmed death ligand 1 (PD-L1), and cytotoxic T-lymphocyte associated protein 4 (CTLA4) antagonist antibodies for multiple advanced solid tumors, have marked a new era of cancer therapeutics that will increasingly harness a patient's immune system to kill and control malignancy (1). The PD-1 receptor on cytotoxic T cells suppresses their activity when bound by its ligands PD-L1 or PD-L2 (2, 3). Disruption of this negative signal using anti–PD-1 or anti–PD-L1 antibodies unleashes T-cell effector properties that lead to tumor cell killing. Similarly, blockade of the T cell–inhibitory molecule CTLA4 stimulates tumor antigen-specific immune responses by suppressing inhibitory signals on naïve T cells and through elimination of regulatory T cells (4).

PD-1 axis antagonist antibodies in non–small cell lung cancer (NSCLC) can induce durable antitumor responses (median duration of response, 12–25 months; refs. 5–12), with some responses lasting well beyond 5 years (13). The longest follow-up study of patients with NSCLC treated with such therapy to date showed an unprecedented 16 percent 5-year survival rate among patients with pretreated advanced NSCLC (13). Currently, the anti–PD-1 agent pembrolizumab is approved for use as first- and second-line therapy in patients with advanced NSCLCs whose tumors express PD-L1 using IHC (10, 11). The PD-1 axis blockers nivolumab (anti–PD-1) and atezolizumab (anti–PD-L1) are additionally indicated for use as second-line therapy in patients with NSCLC regardless of tumor PD-L1 expression (6, 8). Anti-CTLA4–directed therapies, like ipilimumab and tremelimumab, have shown limited activity as single agents in lung cancer (14, 15). However, early-phase studies using the combination of CTLA4 and PD-1 axis inhibitors in patients with advanced NSCLC have shown encouraging results (16, 17). Despite the impressive activity of PD-1 axis inhibitors in some patients with advanced NSCLC, most patients will not benefit from therapy, and the majority of those who respond will ultimately develop drug-resistant tumors.

Little is known about mechanisms mediating primary and acquired resistance to ICIs in lung cancer. Low nonsynonymous mutation burden has been associated with primary resistance to these therapies in melanoma and lung cancer (18–20). In NSCLC, tumors with nondetectable PD-L1

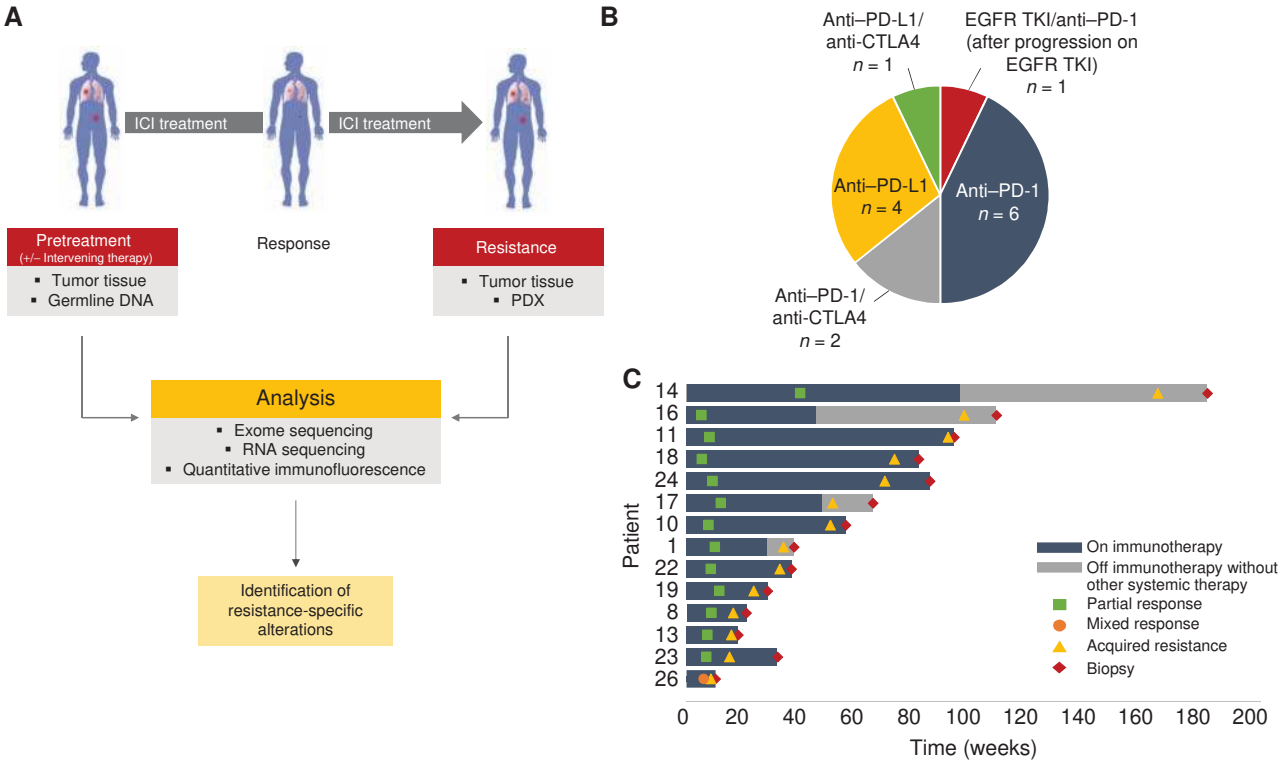

Figure 1. Analytic process and characteristics of the cohort of cases of acquired resistance to ICIs. **A,** Schematic representation of the repeat biopsy program and sample analysis. Tumor specimens (and corresponding PDXs when available) collected at the time of resistance to ICIs and before treatment with ICIs along with germline DNA were analyzed using whole-exome sequencing. For select samples with sufficient material, RNA sequencing and quantitative immunofluorescence were also performed. **B,** Pie chart illustrating the types of therapies received by patients in this study. **C,** Swimmer's plot indicating time of response, resistance to ICIs, and length of time on therapy for individual patients.

expression are also less responsive to these agents, although there is variability depending on the biomarker used (6, 8, 10). Whether these factors are also involved in acquired resistance to ICIs has not been established. In lung cancer, to date, neoantigen loss has been associated with acquired resistance to immune checkpoint blockade (21). In melanoma, acquired resistance to PD-1 inhibitors can be mediated by tumor cell–autonomous defects in interferon (IFN) signaling through *JAK1/2*-inactivating mutations or defective HLA Class I antigen processing through deleterious mutations in Beta-2 microglobulin (*B2M*; ref. 22). Further underscoring the importance of these pathways for resistance to ICIs, defects in the IFN signaling pathway have also been found in melanomas with primary resistance to ipilimumab and pembrolizumab (23), and *B2M* mutations were recently found in metastatic colon cancers resistant to pembrolizumab (24).

To establish whether IFN signaling and HLA Class I antigen processing and presentation machinery (APM) alterations contribute to acquired resistance to ICIs in lung cancer, we investigated the genomic, transcriptomic, and inflammation landscape of lung tumors no longer responsive to ICI using both human lung cancer tissue and tumors grown as xenografts. Here, we describe findings from analysis of 14 cases of lung tumors resistant to ICIs, including 10 cases with available paired pretreatment tumor samples.

RESULTS

The Genomic Landscape of ICI-Resistant Tumors

To identify cellular and molecular mechanisms associated with acquired ICI resistance, we analyzed ICI-resistant NSCLCs collected systematically at our institution between 2011 and 2016 as part of a repeat biopsy program focused on thoracic malignancies. We performed whole-exome DNA sequencing on available tumor samples collected from 14 patients at the time of resistance to PD-1 axis inhibitors, given either alone (n = 10), in combination with a CTLA4 inhibitor (n = 3), or with the tyrosine kinase inhibitor erlotinib after progression on erlotinib alone (n = 1; Fig. 1A and B). For three of the cases, we successfully established patient-derived xenografts (PDX) from the ICI-resistant samples that were also analyzed with whole-exome sequencing (WES). Additionally, RNA sequencing and quantitative immunofluorescence were performed on select specimens for which sufficient material was available. Eleven of the 14 cases demonstrated partial response (PR) per RECIST v1.1 upon treatment with ICIs before developing resistance while on therapy or less than 8 weeks after discontinuing therapy (here classified as "acquired resistance"; Fig. 1C). The remaining cases include two patients who initially responded to ICIs and then recurred more than 8 weeks after discontinuation of therapy (classified as "off-therapy recurrences") and one patient who exhibited simultaneous regression and progression in

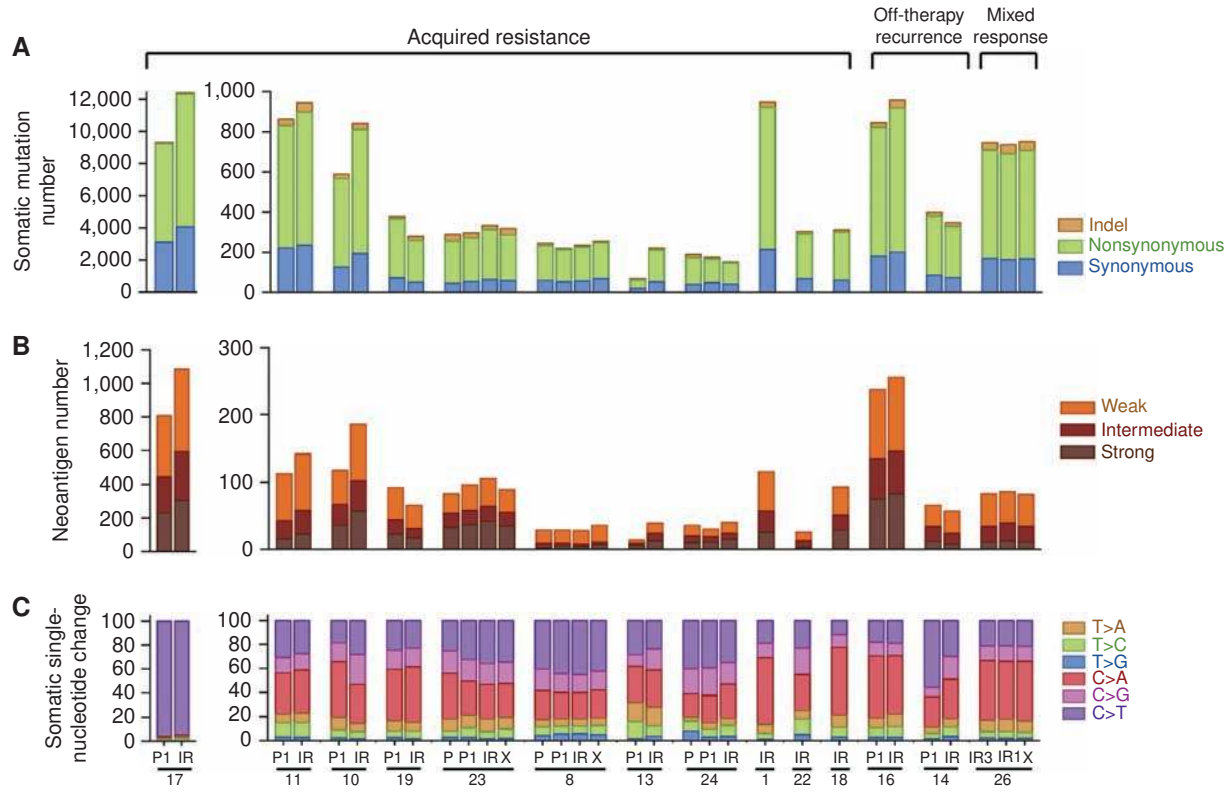

Figure 2. Mutational landscape of acquired resistance to ICIs. Bar graphs showing the (**A**) somatic mutation burden, (**B**) neoantigen burden, and (**C**) mutational signatures in preimmunotherapy specimens (P, P1), immunotherapy resistant specimens (IR), and xenografts (X).

different tumor sites (classified as "mixed response"). The cohort included squamous ($n = 6$), nonsquamous ($n = 7$), and mixed squamous/nonsquamous ($n = 1$) NSCLC; 4 tumors harbored mutations in major oncogenic drivers (Supplementary Table S1). Twelve patients had a ≥15 pack-year smoking history. In the 11 acquired resistance cases, the median time to resistance was 236 days (33.7 weeks; Fig. 1C). In the two patients with off-therapy recurrences, progression developed 361 and 482 days (51.6 and 68.9 weeks) after discontinuation of the ICI.

The median number of overall somatic mutations per sample in the pretreatment specimens was 389 (range, 68–9,302; Fig. 2A). Of note, the median number of somatic mutations found in the pan–lung cancer analysis of data from The Cancer Genome Atlas (TCGA) was 261, and 327 in a separate study of metastatic lung cancers (18, 25). This difference likely reflects the inclusion in our cohort of cases of metastatic lung cancer (as opposed to resectable cases included in the TCGA dataset) and of tumors that responded to ICIs (18). First, we investigated whether the number of somatic nonsynonymous (NS) mutations changed between pre- and ICI-resistant tumors. For this analysis, we studied 8 of the 11 acquired resistance cases that had paired pretreatment tumor material available (Fig. 2; the off-treatment relapses and mixed response cases were not included in these analyses to minimize potential confounding variables). One of these cases (#17) exhibited a hypermutator phenotype with >6,000 nonsynonymous mutations per tumor. Although our study was underpowered to conclusively establish whether the mutation load of tumors changed at acquired resistance, we found increased mutation load in 6 of 8 paired cases that harbored NS mutation burdens ranging from 74% to 356% of those of the pretreatment sample (Fig. 2A).

To evaluate the hypothesis that antigenicity of the tumor may be altered in ICI-resistant samples, we calculated the number of *in silico* HLA-restricted (i.e., that match the person's HLA profile) predicted HLA Class I neoantigens in tumor samples. As expected, the number of candidate neoantigens generally correlated with the number of somatic mutations (Pearson correlation r of 0.98, $P < 0.0001$). Similar to the NS mutation burden, when we examined the 8 individual pairs of pre- and acquired resistance cases, the number of neoantigens in the ICI-resistant specimens ranged from 71% to 278% of the number in pretreatment specimens and increased in 6 of 8 pairs (Fig. 2B). We then examined the predicted binding affinities for HLA I alleles of the candidate neoantigens identified in the tumor specimens. Overall, the distribution of neoantigens predicted to have strong, intermediate, and weak binding affinities (strong: $IC_{50} \leq 50$ nmol/L; intermediate: 50 nmol/L $< IC_{50} \leq 150$ nmol/L; weak: 150 nmol/L $< IC_{50} \leq 500$ nmol/L) for their corresponding HLA I alleles was similar in pretreatment and ICI-resistant specimens (Supplementary Figs. S1A and S1B).

Next, we sought to identify mutational signatures in the whole-exome sequence data from the complete cohort dataset (Fig. 2C). Our analysis revealed that in the majority of the tumor specimens the dominant mutation signatures

were those associated with smoking, APOBEC mutations, and to a lesser extent alkylating agents (refs. 26, 27; Supplementary Fig. S2A). With the exception of two paired cases (#10, acquired resistance; #14, off-therapy recurrence), the predominant pattern present in the pretreatment specimen was retained in the patient-matched, resistant tumor specimen (Supplementary Fig. S2B). The hypermutator case identified in our cohort (case #17) exhibited a mutation signature rich in C>T transitions suggestive of exposure to an alkylating agent (26). Indeed, the patient received temozolomide during the course of therapy prior to treatment with an ICI.

Acquired *B2M* Loss upon Acquired Resistance to ICIs

Defects in HLA Class I antigen processing and presentation have been documented in cases of resistance to several immunotherapies, including IL2, tumor-infiltrating lymphocyte adoptive cell therapy, and in one melanoma and two colorectal cancer cases of acquired resistance to pembrolizumab (22, 24, 28–30). To establish whether genetic defects in genes encoding HLA Class I APM components were found at resistance to ICIs in our cohort, we surveyed 72 genes involved in antigen processing and presentation (http://www.genome.jp/dbget-bin/www_bget?hsa04612). Overall, recurrent mutations and/or copy-number alterations in genes in this pathway were not found in the ICI-resistant specimens, although we identified several genes with acquired mutations, including *PSMD13, CD207, PSMD4, PSMD7*, and *PSMD1* (Fig. 3; Supplementary Table S2). Copy-number variation analysis showed homozygous loss of *B2M* in one case of acquired resistance to therapy (case #23) and heterozygous loss in a second case after progression off therapy (case #14). Given the strong genetic evidence for progressive loss of *B2M* in case #23 and the well-established role of B2M in HLA Class I antigen processing and presentation, we decided to further investigate the case with homozygous acquired *B2M* loss. The patient (case #23), a 75-year-old woman with stage IV squamous cell carcinoma of the lung, received first-line systemic therapy with carboplatin and gemcitabine, and second-line therapy with docetaxel. Upon progression with docetaxel, she initiated clinical trial therapy with a PD-L1 antibody combined with a CTLA4 antagonist antibody (Fig. 4A). She experienced rapid clinical improvement and radiographic regression at all sites of disease, including extensive mediastinal and hilar adenopathy (Fig. 4A). Trial imaging after 4 months of therapy identified a new celiac mass, which revealed itself to be a cancerous lymph node, while the patient had sustained response at known sites of disease (Fig. 4A). This mass was laparoscopically resected, revealing a lymph node infiltrated with squamous cell carcinoma, and she continued a one-year course of immunotherapy without further disease progression. Her disease recurred after nine months without systemic therapy, with mediastinal, cervical, and retroperitoneal adenopathy. She restarted anti–PD-L1 and anti-CTLA4 therapy with marked second response by CT and PET imaging. Histopathologic analysis of the tumor specimen collected immediately prior to initial ICI therapy demonstrated moderately differentiated squamous cell carcinoma with no discernible PD-L1 expression on tumor cells, although rare PD-L1 expression was appreciated on immune cells present in the tumor (Fig. 4B). Considering that the celiac mass represented an involved lymph node, characterization of infiltrating and surrounding immune cells was limited. Of note, an earlier pre-chemotherapy diagnostic specimen from a lung biopsy demonstrated a highly inflamed tumor that also did not express PD-L1 on tumor cells. The on-treatment excised celiac mass specimen demonstrated tumor involvement of lymph nodes, with sheets of squamous cell carcinoma cells separated by areas of uninvolved lymphoid tissue (Fig. 4C). Notably, similar to the specimen harvested immediately before ICI treatment ("pre-immunotherapy"), morphologic evaluation of the histologic specimen stained with an anti–PD-L1 antibody from the resistant sample did not detect PD-L1 on tumor cells, but showed increased PD-L1 expression in surrounding immune cells relative to the pre-ICI specimen (Fig. 4C). Copy-number variation analysis of paired WES data revealed homozygous *B2M* loss in the ICI-resistant specimen (Fig. 4D). Of note, the diagnostic pre-chemotherapy specimen had both copies of *B2M*, but harbored a subclonal (non-reference allele frequency of 10%) deleterious mutation in *B2M* (p.M1I) that was not found in subsequent specimens. Only one copy of *B2M* was found in the pre-immunotherapy specimen (Fig. 4D). These findings were further confirmed using quantitative real-time PCR (Supplementary Fig. S3). To evaluate the levels of B2M and HLA Class I protein directly in the patient's specimens, we used multiplexed quantitative immunofluorescence (see Supplementary Methods for details). Consistent with the genomic data for case #23, we found a statistically significant reduction in the level of B2M on the cytokeratin-positive tumor cells in the immunotherapy-resistant specimen compared with the tumor sampled prior to immunotherapy (Figs. 4E and F, $P < 0.0001$). Analysis of the levels of HLA I (using the HC-10 antibody that detects select HLA-A types, HLA-B and HLA-C molecules) revealed reduced levels of HLA Class I in the acquired resistance sample (Supplementary Fig. S4A and S4B). We also analyzed the levels of B2M and HLA Class I in the stromal (cytokeratin-negative) compartment. We found that the levels of B2M were also downregulated in the stromal compartment at acquired resistance. This could

Figure 3. The genomic landscape of antigen processing and presentation pathway genes. Oncoprint generated from whole-exome sequencing data from 13 cases. Only genes with alterations are shown. Mutated genes are listed vertically in order of frequency of somatic single-nucleotide mutations or copy-number alterations in the preimmunotherapy cases. A case with a hypermutator phenotype (#17) sample was excluded from this analysis. Preimmunotherapy specimens are shown on the left and immunotherapy-resistant tumors on the right. *Of note, sample 26-IR1 was collected from a site (adrenal metastasis) that responded to a short course of ICI, but progressed during a 2-month delay of treatment when steroids were administered for cerebral edema associated with new intracranial disease (sample 26-IR3) and pneumonitis. This site subsequently regressed with reintroduction of ICI.

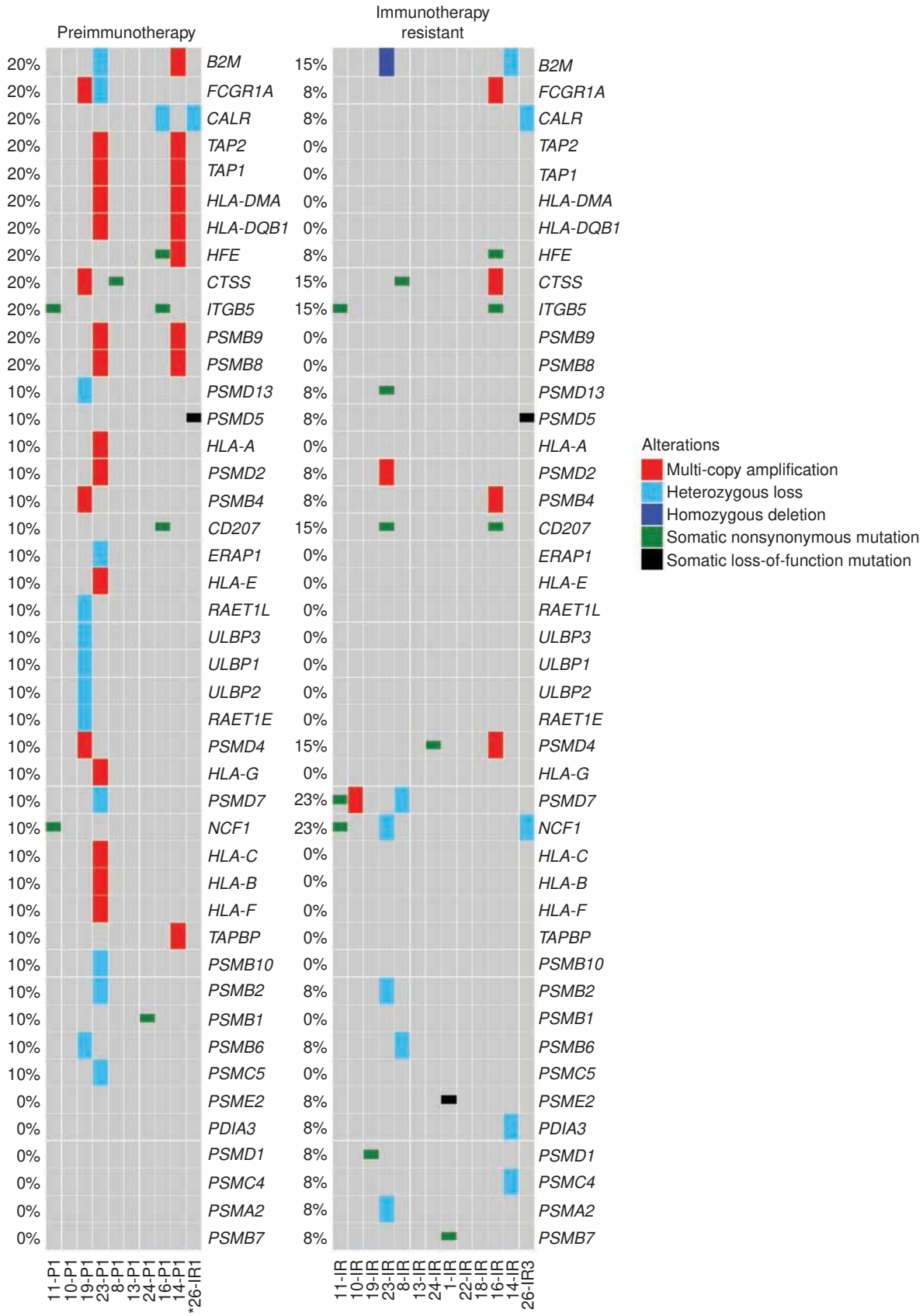

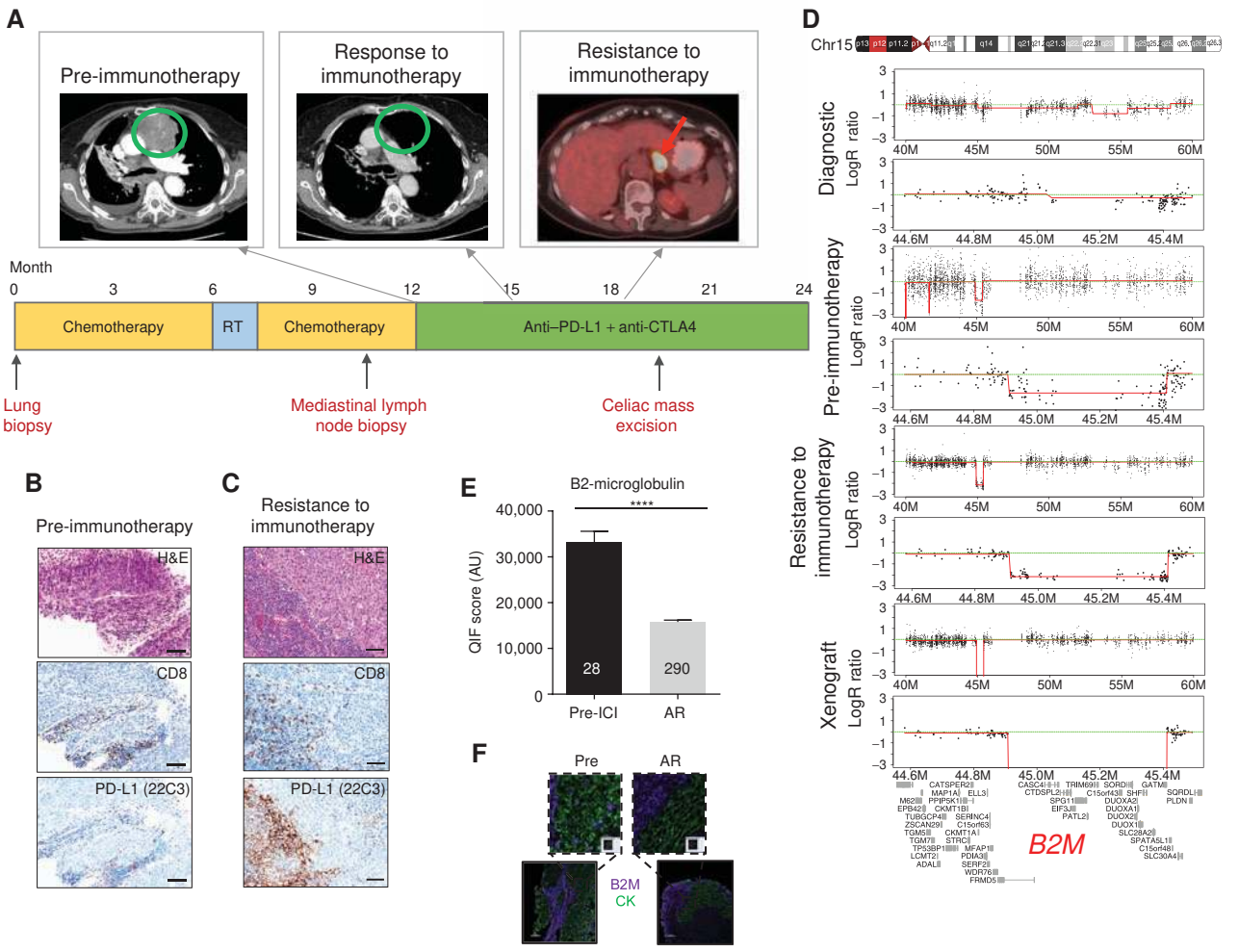

Figure 4. *B2M* loss in a case of acquired resistance to immunotherapy. **A,** Treatment timeline for case #23. After receiving palliative thoracic irradiation and two lines of standard chemotherapy, the patient initiated trial therapy with anti–PD-L1 and anti-CTLA4 agents. First on-trial imaging assessment demonstrated partial response (see green circles). Imaging after 4 months of therapy showed a new celiac mass (red arrow) with sustained response at known sites of disease. After resection of this mass, this patient continued trial therapy, completing the prescribed one-year course, during which the patient had no further progression of disease. **B** and **C,** Hematoxylin and eosin (H&E), CD8, and PD-L1 immunohistochemical staining of the tumors before treatment and at acquired resistance to anti–PD-L1 and anti-CTLA4 blockade. Scale bars, 250 μm. **D,** Copy-number variation analysis of paired tumor specimens and a PDX derived from the immunotherapy-resistant tumor specimen revealed acquired homozygous loss of *B2M* at the time of acquired resistance to anti–PD-L1 and anti-CTLA4 blockade. **E** and **F,** Multiplex quantitative immunofluorescence (QIF) of B2M in pre-immunotherapy and immunotherapy-resistant tumor tissues from case #23. **E,** Bar graph depicting the levels of B2M in whole tumor sections from pre-immunotherapy and immunotherapy-resistant samples measured using multiplex quantitative immunofluorescence and quantified with AQUA software. Numbers in the individual bars represent total fields of view analyzed. Statistical significance was calculated using the Mann–Whitney test. ****, $P < 0.0001$. AU, arbitrary units. **F,** Multiplex immunofluorescence image representing one field-of-view (FOV), showing the expression of B2M (purple) specifically in the tumor compartment represented by cytokeratin positive epithelial cells (green) and nuclear staining with DAPI (blue) respectively. Scale bar, 100 μm. AR, acquired resistance; CK, cytokeratin; RT, radiation therapy.

reflect the presence of lower levels of IFNγ in the absence of a less-abundant and activated T-lymphocyte infiltrate. HLA Class I levels, however, were upregulated in the stroma (Supplementary Fig. S4C and S4D, $P < 0.0001$) at acquired resistance to checkpoint blockade. The functional importance of these findings remains to be determined.

To further investigate the extent to which reduced B2M levels and consequent reduced levels of cell surface HLA Class I are observed in tumors at acquired resistance to ICIs, we surveyed 3 PDX models derived from specimens that were resistant to ICIs and included in our cohort (cases #8, #23, and #26) and two additional models derived from tumors with primary resistance to immune checkpoint blockade not included in the cohort (cases #7 and #3; see Supplementary Table S1). Consistent with our copy-number analysis, the PDX derived from case #23's ICI-resistant tumor showed total B2M protein loss. Although the other 4 PDXs generated had evidence of B2M expression, the levels of B2M were low in the PDXs derived from cases #26 and #7 (Fig. 5A). Consistent with the Western analysis, using flow cytometry to analyze PDX-derived tumor cells, we found a lack of B2M expression on the case #23–derived PDX and low levels of the protein on PDX-derived cases #26 and #7 in contrast to cases #3 and #8 (Fig. 5B). We did not detect HLA Class I

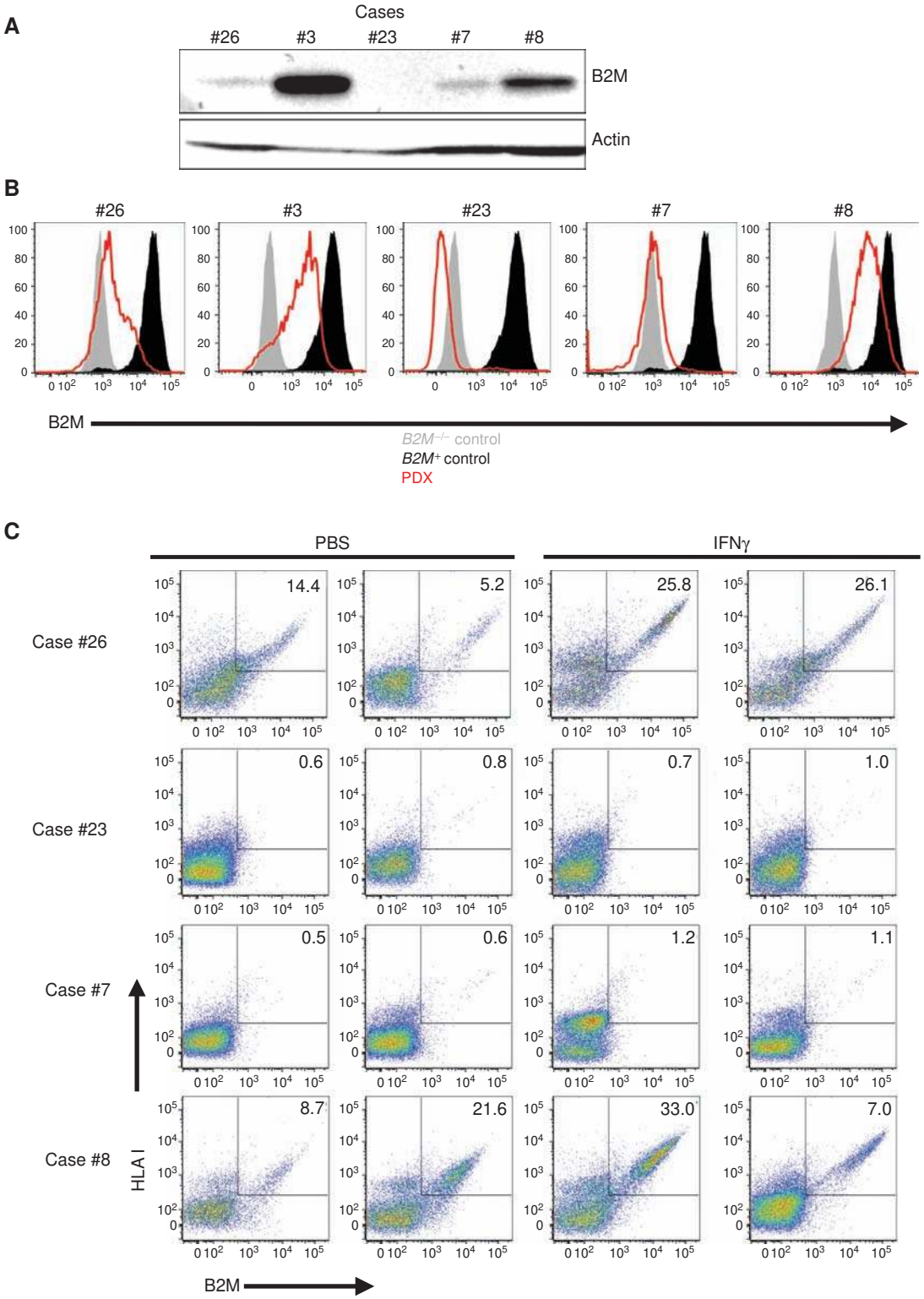

Figure 5. Defects in HLA Class I antigen processing and presentation in ICI-resistant tumors following *B2M* loss. **A,** Western blot analysis showing the absence of B2M protein expression in a PDX from case #23 generated at the time of acquired resistance to anti–PD-L1 and anti-CTLA4 blockade. Also shown is B2M protein expression in 4 PDXs established from other patients with tumors resistant to PD-1 pathway blockade (cases #26, #3, #7, and #8). **B,** Flow-cytometry analysis for expression of B2M on PDX samples from cases #26, #3, #23, #7, and #8. **C,** Flow-cytometry analysis of PDXs derived from cases #26, #23, #7, and #8 for B2M and HLA-I cell-surface expression following intratumoral injection of either PBS or IFNγ. Each flow plot represents an independent mouse tumor used for these studies.

expression by flow cytometry in cases #23 and #7 (Fig. 5C), therefore indicating the inability of these tumors to present tumor antigen-derived peptides to cognate T cells. To determine whether the HLA Class I downregulation found in these cases was caused by defects in the IFNγ pathway, we performed intratumoral injections of human IFNγ into established PDX tumors, and then we examined tumors for IFNγ pathway activation by measuring the levels of phosphorylated STAT1 (pSTAT1) and B2M by Western blot and B2M-associated HLA Class I heavy chain expression by flow cytometry. As expected, case #8, which had robust baseline B2M expression, showed increased pSTAT1 and increased numbers of cells expressing B2M and cell-surface HLA Class I in the CD45-negative fraction of the tumor preparation following IFNγ treatment (Fig. 5; Supplementary Fig. S5). In the case with *B2M* genomic loss (case #23), STAT1 phosphorylation increased without increases in either B2M or HLA Class I upon IFNγ stimulation (Supplementary Fig. S5). In the two cases with low baseline B2M, we found that both pSTAT1 and B2M were increased following IFNγ treatment (Supplementary Fig. S5). However, in only one (case #26) was this accompanied by increased cell-surface HLA Class I in CD45-negative cells, suggesting that responsiveness of the tumor to IFNγ was intact (Fig. 5C). In case #7, we did not observe a robust increase in HLA Class I antigen expression on tumor cells, suggesting that this tumor lacks the ability to fully respond to IFNγ (Fig. 5C).

Next, we surveyed the panel of pre-ICI and ICI-resistant cases for which sufficient tissue was available (8 acquired resistance and 1 post-therapy relapse) in our cohort for B2M and HLA Class I protein levels, specifically in cytokeratin-positive tumor cells using multiplexed quantitative immunofluorescence. We found significantly reduced levels of HLA Class I (4/9 cases) and B2M (3/9 cases) at resistance, including case #23 (Supplementary Fig. S6). Notably, we could also detect increased expression of HLA Class I and/or B2M in tumor cells in some acquired resistance cases (i.e., cases #10, #11, #19, #24, #17, and #16) at acquired resistance, which could be related to enhanced (and possibly futile) immune activation induced by the ICI.

B2m Loss Confers Resistance to Anti–PD-1 Therapy *In Vivo* in an Immunocompetent Syngeneic Model

To further explore the role of B2M in mediating resistance to immune checkpoint inhibition, we examined the level of B2M protein in a murine carcinogen-induced lung cancer cell line, UNSCC680AJ, which has been shown to be sensitive to anti–PD-1 therapy (31). To test if B2M expression affects sensitivity to checkpoint inhibitors *in vivo*, we used CRISPR-mediated techniques to knockout *B2m* in this cell line (Fig. 6A). We injected *B2m* wild-type or *B2m* knockout UNSCC680AJ cells into the flanks of syngeneic immunocompetent A/J mice. When the tumor volumes reached approximately 30 mm^3, mice were randomized to receive either anti–PD-1 or isotype control antibody. UNSCC680AJ tumors with intact *B2m* responded to anti–PD-1 treatment, whereas tumors composed of *B2m* knockout cells progressed through PD-1 blockade (Fig. 6B). Because an important aspect of antitumor CD8 T cells is the ability to kill target tumor cells (32), we assessed the cytotoxicity of UNSCC680AJ tumor-specific CD8 T cells toward both the control (empty vector) and the *B2m* knockout UNSCC680AJ tumor cell lines. A significant defect in the overall killing of *B2m* knockout cells, in particular at the highest effector/target ratio (1:1; Fig. 6C), was observed. Furthermore, we did not see appreciable cytotoxicity of either UNSCC680AJ cell line in the presence of splenic CD8 T cells (Fig. 6D), suggesting that the observed cytotoxicity is tumor specific.

Genomic Alterations in IFN Signaling in Resistant Tumors

Because genetic defects in IFN pathway–related genes have been associated with primary and acquired resistance to ICIs, we compiled a list of 101 IFN pathway–related genes (33) and queried them for mutations and copy-number alterations in our cohort (excluding the hypermutator, case #17, that was examined separately; Supplementary Fig. S7). Acquired missense mutations were identified in *IFNAR2, TYK2, IL15, IL2RB*, and *IFIH1* (Supplementary Table S3). All of these mutations had a <30% allelic frequency, suggesting that they were heterozygous mutations. The functional significance of these alterations is unclear. Indeed, with the exception of the A540V mutation in *IFIH1*, S49T mutation in *IL2RB* (we found an S49I mutation in our cohort), and N58fs in *IFNAR2* (we found an N58K mutation in our cohort), the specific missense mutations are not found either in the Catalogue of Somatic Mutations in Cancer (COSMIC) or in cBioPortal. The resistant specimen from the hypermutator case #17 also had several acquired mutations in the IFNγ pathway (Supplementary Table S3). Notably, we found a mutation in *JAK1* at a residue encoding the SH2 domain of the protein (P429L) that had a ~50% allele frequency. When we adjusted for tumor purity and recalculated the predicted allele frequency of the mutation, it increased to 67%. Adjacent residues 430 and 431 are frameshift mutation hotspots in this gene in several types of cancer (www.cbioportal.org), and a P429S mutation was recently described in a melanoma with primary resistance to immune checkpoint blockade that had a defective response to induction with type I and type II interferons (23). We did not find additional JAK1/2 mutations in our cohort.

An Inflammatory Microenvironment Is Present at Acquired Resistance to Immunotherapy

To further explore mechanisms of resistance to ICIs, we performed RNA sequencing on seven paired cases in our cohort with sufficient tissue which included case #23 (with *B2M* loss). Broad upregulation of immune inhibitory receptor genes was appreciated at resistance, including genes encoding LAG3, PD-1, TIGIT, 2B4, CTLA4, and to a lesser extent TIM3 (Fig. 7A). The increase in LAG3 was statistically significant (Fig. 7A, $P < 0.05$). Interestingly, although the expression of PD-L1 remained unchanged upon resistance to immune checkpoint blockade, PD-L2 expression increased on average 7.7-fold in these resistant specimens (Fig. 7B). Additionally, although receptors responsible for T-cell activation were generally upregulated in the resistant specimens (Fig. 7A), we observed that

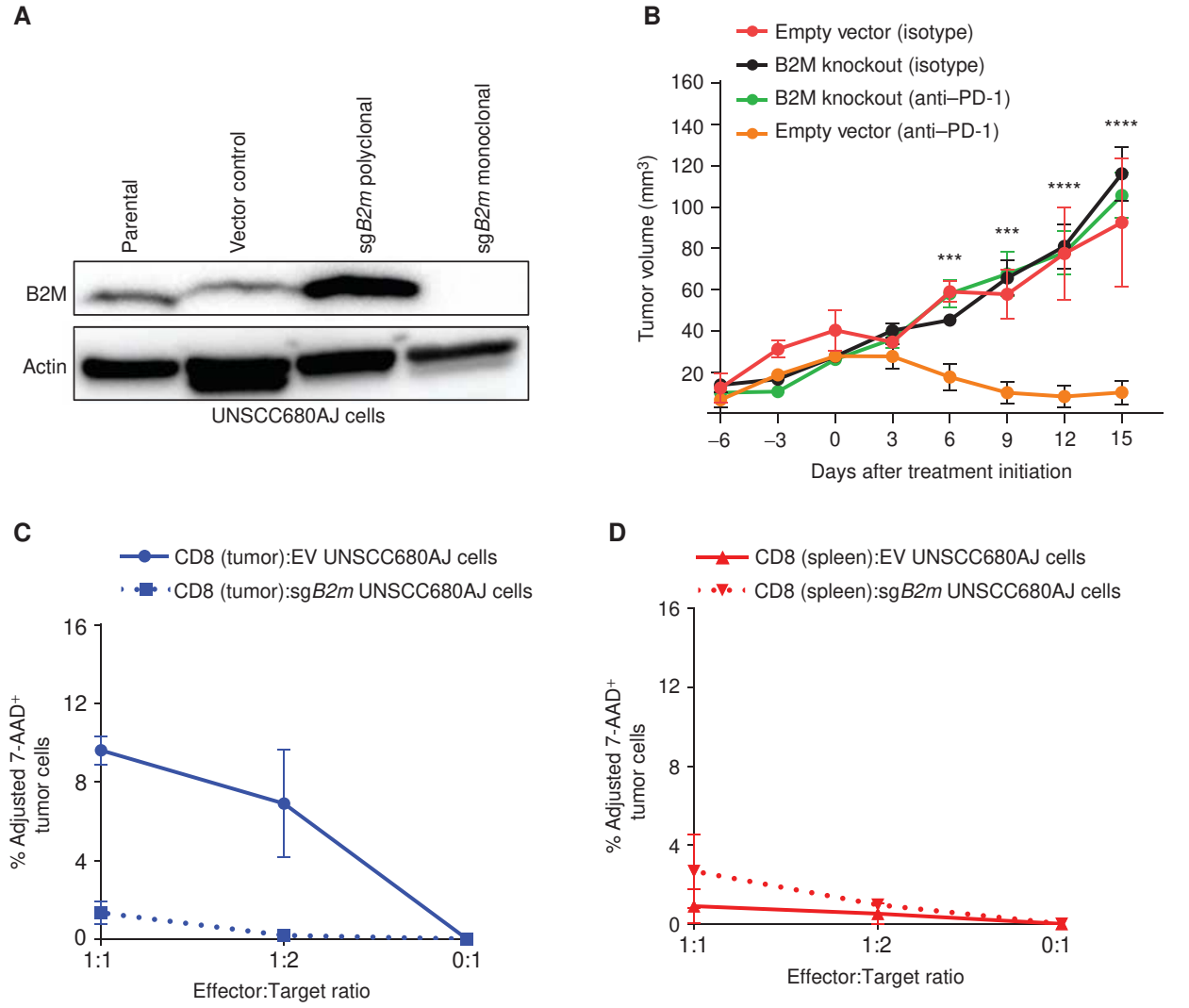

Figure 6. *B2m* loss confers resistance to anti–PD-1 therapy and impairs CD8 cytotoxicity *in vivo* (**A**) Western blot analysis of B2M expression in UNSCC680AJ lung cancer cells transfected with a plasmid expressing Cas9 and a sgRNA targeting *B2m* (*sgB2m* polyclonal). Additionally, single-cell sorting identified clonal populations where B2M expression was absent (*sgB2m* monoclonal). **B,** 5×10^5 UNSCC680AJ cells from the monoclonal B2M-null population and vector control cells were injected into the dorsal flanks of A/J mice subcutaneously. Tumors were allowed to grow to approximately 30 mm^3 before administration of 100 μg of anti–PD-1 or isotype control via intraperitoneal injection every 3 days. Tumors were measured every 3 days with a caliper, and tumor volumes were calculated. Data are presented as the mean tumor volume ± SEM. The size of the tumors in the *B2m* wild-type and *B2m* knockout lines treated with anti–PD-1 were compared at the indicated time points using a *t* test. ***, $P < 0.001$; ****, $P < 0.0001$. Additionally, cytotoxicity assays were performed to assess the percentage of viable target cells [empty vector (EV) UNSCC680AJ or sg*B2m* UNSCC680AJ] after coculturing the cell lines *in vitro* with EV UNSCC680AJ tumor-infiltrating CD8 T cells (**C**) or T cells from the spleen (**D**). Data represent $n = 2$ mice, with error bars denoting standard error of the mean.

gene expression in four of five corresponding T cell–activating ligands we examined, including 4-1BB-L, ICOS-L, OX40-L, and CD40-L, was unchanged or downregulated at resistance (Fig. 7B). This analysis also revealed increased expression of CD8 T-cell effector molecules at resistance, including GZMB ($P < 0.05$), TNFα, and IFNγ (Fig. 7C). To establish whether these findings were observed at the protein level, we performed multiplexed quantitative immunofluorescence on matched tumors with available tissue from eight cases for localized measurements of the immune inhibitory receptors PD-1, LAG3, and TIM3 and seven matched cases for the T-cell activation markers Ki-67 and GZMB in $CD3^+$ T lymphocytes. Consistent with the RNA-sequencing data, we found upregulation of PD-1 and LAG3 in five of eight cases examined, whereas TIM3 levels were increased in only three of eight cases at acquired resistance (Fig. 7D and E; Supplementary Fig. S8). In most cases, Ki-67 was uniformly upregulated in T cells in the acquired resistance specimens compared with pretreatment cases, whereas GZMB showed a more variable pattern (Fig. 7F and G). Overall, these data support the presence of a more inflammatory microenvironment in tissues following treatment with the ICIs compared with pretreatment specimens.

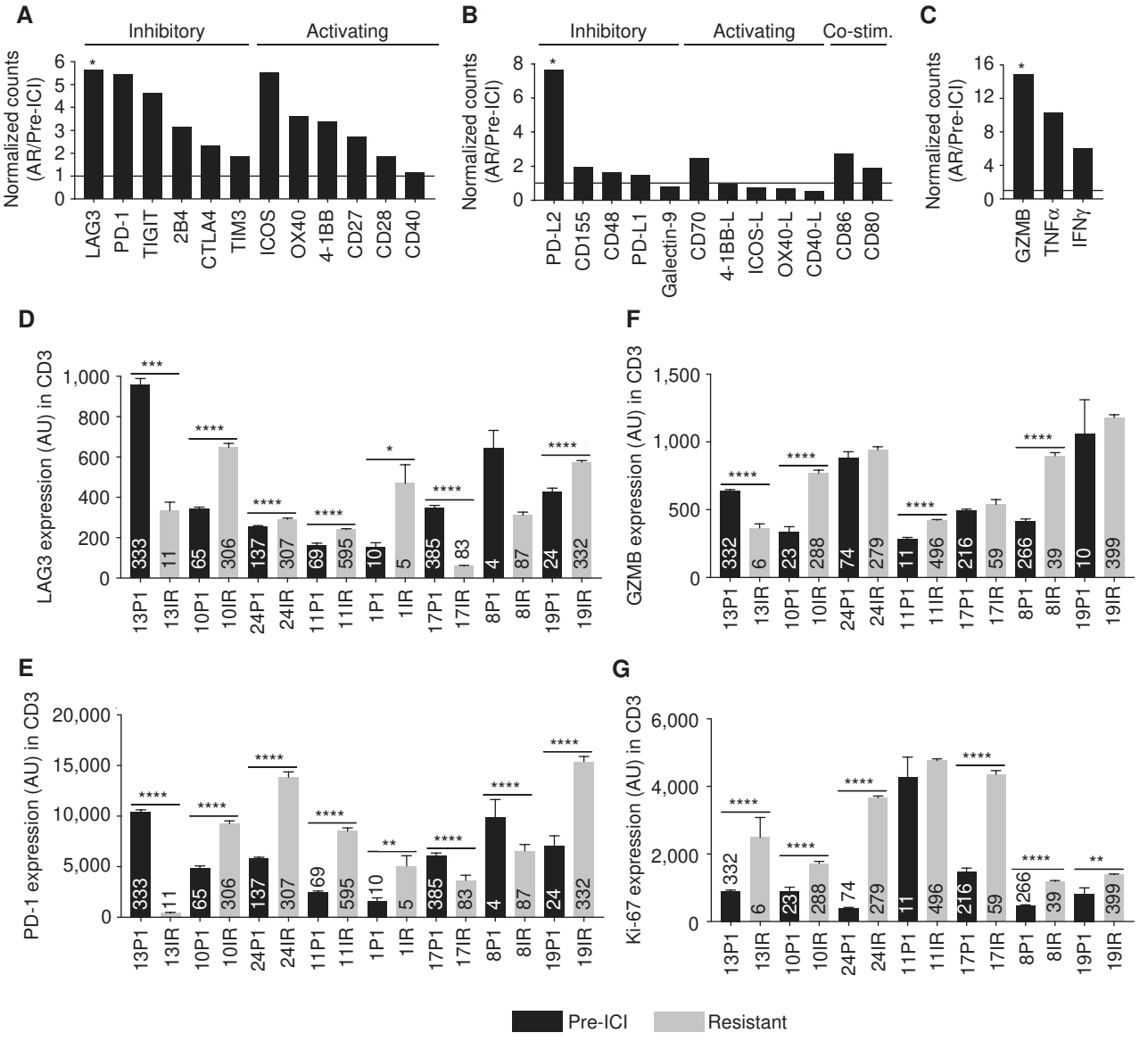

Figure 7. RNA sequencing and tumor immunoprofiling of T cell–inhibitory and activation markers in tumor tissues from patients pre-immunotherapy and at resistance to ICIs. Ratio of normalized RNA sequencing–derived read counts of T cell–inhibitory and activating receptors (AR; **A**), ligands (**B**), and effector molecules (**C**) in immunotherapy-resistant specimens ($n = 7$) compared with pre-immunotherapy specimens ($n = 4$). **D–F,** Quantitative immunofluorescence analysis showing the levels of the immune-inhibitory molecule LAG3 (**D**), the T-cell exhaustion marker PD-1 (**E**), T-cell activation effector molecule Granzyme B (GZB; **F**) and T-cell proliferation marker Ki-67 (**G**) in CD3-positive tumor-infiltrating lymphocytes (TIL) in paired pre- and post-immunotherapy tumor samples as quantified using the AQUA software. Numbers in the individual bars represent total fields of view analyzed. Statistical significance was calculated using the Mann–Whitney test. P1, pre-immunotherapy; IR, immunotherapy resistant. ****, $P < 0.0001$; ***, $P < 0.001$; **, $P < 0.01$; *, $P < 0.05$.

DISCUSSION

Approximately 20% of unselected patients with advanced NSCLC will respond to either PD-1 or PD-L1 inhibition, and studies to explore ways to overcome primary resistance are ongoing. However, of equal importance, the majority of patients who initially benefit from these therapies eventually develop drug-resistant disease. Currently, we have a limited understanding of the mechanisms that enable such resistance in lung cancer. By analyzing serial tumor specimens from patients with NSCLC who have acquired resistance to PD-1 axis inhibitors, we report the first example of impaired HLA Class I antigen processing as a mechanism of acquired resistance to ICIs. In one case presented here, we identified homozygous *B2M* loss in a tumor that had acquired resistance to combined anti–PD-L1 and anti-CTLA4 therapy. B2M is an essential component of the HLA Class I complex, and tumor B2M deficiency (or defective cell surface HLA I expression) has been implicated in immune escape and as a negative prognostic factor in several types of cancers (34–39).

It has additionally been implicated as a mechanism of resistance to immunotherapies, including T cell–based therapies and vaccination in patients with advanced melanoma (29, 40). Recently, a case of advanced melanoma with acquired resistance to the anti–PD-1 antibody pembrolizumab, presumably mediated by *B2M* deficiency, was reported (12). This patient's resistant tumor harbored a homozygous *B2M*-truncating mutation, with loss of cell-surface HLA Class I expression. Additionally, B2M alterations were also described in two ICI-resistant brain metastases from patients with mismatch repair–deficient colorectal cancer (24). In our case, we detected a deleterious *B2M* mutation in the diagnostic specimen (at low allelic frequency), which was lost during treatment with chemotherapy, at which point heterozygous loss of the gene was detected. Total *B2M* loss at the time of acquired resistance to ICI therapy was subsequently identified. Supporting this mechanism, we demonstrate ICI therapy resistance induced by CRISPR-mediated *B2m* knockout in an immunocompetent lung cancer mouse model. Beyond *B2M* homozygous loss, we did not find clear evidence of additional individual alterations that impair HLA Class I antigen processing and presentation. However, we did find multiple heterozygous mutations or monoallelic copy-number variations (CNV) in tumors in this pathway in our cohort. Further studies to establish the consequences of these alterations on HLA Class I antigen processing and presentation are ongoing. One hypothesis is that although none of these events alone are sufficient to downmodulate antigen presentation, multiple hits together in the same pathway could have this effect, similar to how hemizygous loss of multiple contiguous tumor suppressor genes can affect tumorigenesis (41, 42). Further supporting the potential for a role of defective antigen processing and presentation defects in mediating resistance to ICIs, we found that three out of five PDXs generated from ICI-resistant tumors exhibited B2M downregulation, and two of these also had either loss or barely detectable levels of cell-surface HLA Class I expression. However, genomic *B2M* loss was found in only one of the cases studied, suggesting that additional genomic or nongenomic mechanisms beyond *B2M* loss can lead to HLA Class I downregulation and may contribute to resistance to ICIs. In particular, epigenetic alterations and activation of signaling pathways that downmodulate cell-surface HLA Class I expression could play a role in resistance to ICIs.

These data support future efforts to comprehensively assess and conclusively establish the contribution of defects in antigen processing and presentation to acquired resistance to ICIs. Moreover, because genetic defects in antigen-processing machinery genes have been found in ~5% of lung cancers and have been linked to reduced survival upon treatment with ICIs (25, 43), the contribution of this pathway to primary resistance in lung cancer should also be considered.

In our study, we functionally demonstrate in an immunocompetent mouse model that knockout of *B2m* confers resistance to immune checkpoint blockade. This experiment serves several purposes. First, it confirms experimentally that tumor cell–autonomous loss of B2M mediates resistance to ICIs. Second, by modeling resistance *in vivo* in an immunocompetent setting, it is now possible to study the molecular and immunologic alterations that occur in tumors with antigen-processing defects. Third, this platform can be used to further investigate the functional role of genomic alterations found in resistant tumors, such as mutations in APM and interferon pathway genes described in Fig. 3 and Supplementary Fig. S7.

Studies of resistance to targeted therapies in lung cancer have revealed that multiple different mechanisms can lead to drug resistance, including mutations in the drug targets, activation of bypass signaling pathways, and alterations in the tumors that render them less dependent on the therapeutic target. A parallel with the latter resistance mechanism can be drawn, in the case of acquired resistance to ICIs, with mutations in the APM or loss of neoantigens, which render the tumors less susceptible to attack by immune cells. This raises the question of whether other similarities with resistance to targeted therapies are observed. We did not find strong evidence of acquired alterations in genes encoding the therapeutic targets in our dataset such as mutations or copy-number variations in *PDCD1, CD274,* and *CD152*. In only the hypermutator (case #17) we found evidence of an acquired missense mutation in *PDCD1*. Whether this is a passenger or a driver mutation in this tumor remains to be determined given the large number of mutations in the sample. Moreover, it is unclear what the consequences of a mutation in *PDCD1*, presumably on tumor cells, would be given that PD-1 is expected to function in T cells, although tumor cell–autonomous functions have been reported (44). We also investigated whether bypass signaling mechanisms via upregulation of compensatory immune inhibitory molecules were found in the resistant tumors. Transcriptomic and immunofluorescence analysis of a subset of the resistant tumors indeed revealed upregulation of several immune-inhibitory receptors, including LAG3, PD-1, TIGIT, 2B4, TIM3, and the PD-L2 ligand, which individually or collectively could account for the resistance in some of the samples. Indeed, upregulation of the immune inhibitory receptor TIM3 on T cells has been described to contribute to adaptive resistance to PD-1 blockade in mouse models and patient specimens (45). Experiments to investigate these scenarios are needed to shed light on the role of these genes and pathways in acquired resistance.

Although this study has limitations, this is one of the largest datasets of ICI-resistant NSCLC tumors reported to date. Because the use of ICIs is relatively recent and responses are usually prolonged, the number of cases that we have analyzed to date is limited. We therefore cannot accurately estimate the fraction of tumors in which defective antigen presentation either through B2M loss or other alterations will contribute to acquired resistance to ICIs. Given the recent approvals of pembrolizumab, nivolumab, and atezolizumab for NSCLC, we anticipate that the number of specimens available for study will increase in coming years, allowing us to address this issue. Another limitation in this study comes from heterogeneity in the sites of tumor sampling. In only one case (#16, an off-therapy recurrence case) was the same tumor site sampled pretreatment and at acquired resistance to ICIs. We therefore cannot exclude that some of the alterations found between pre- and posttreatment specimens are independent of the exposure to ICIs. Furthermore, six of ten patients with paired pre-ICI and ICI-resistant tumor specimens analyzed

had received systemic therapy between pre-ICI specimen collection and initiation of ICI therapy. Hence, acquired alterations potentially attributable to these therapies cannot be excluded. Finally, one of the caveats of this study is that we do not have biopsies from patients' responding sites while they are receiving therapy for comparison, and we therefore cannot determine how the inflammatory milieu found at resistance compares with that observed in a responding tumor.

In conclusion, our study provides the first evidence that defective antigen processing can emerge as a mechanism of acquired resistance to ICIs in lung cancer. Future studies into the frequency with which these defects occur and the underlying mechanisms that lead to them will be important to understand and overcome resistance to these immunotherapies.

METHODS

Patients and Tumor/Blood Specimens

Patients with advanced NSCLC who developed progression to PD-1 axis inhibitor therapy provided consent and were enrolled to a Yale University Institutional Review Board–approved protocol, in accordance with ethical guidelines, allowing the collection and analysis of clinical data, archival and fresh tissue, and blood, and the generation of PDXs. For genomic studies, formalin-fixed paraffin-embedded (FFPE) tissue was macrodissected to enrich for tumor material. All of the tumor samples analyzed had a purity >20% as assessed from the WES data. Patient samples are indicated as "P" for pre-immunotherapy, with "P1" indicating samples collected nearer to initiation of immunotherapy and "IR" for immunotherapy resistant.

WES and Somatic Mutation Analysis

Genomic DNA was captured on the NimbleGen 2.1M human exome array and subjected to 74 base paired-end reads on the Illumina HiSeq2500 instrument. The mean coverage for normal was 103×, and the mean coverage for tumor was 259×. Sequence reads were mapped to the reference genome (b37 build) using BWA-MEM. Sequence reads outside the targeted sequences were discarded, and the statistics on coverage were collected from the remaining reads using in-house perl scripts. Somatic mutations were called by MuTect2. For all somatic mutations called, we extracted base coverage information in all samples and considered the mutations that were supported by at least two sequence reads covering nonreference alleles and present in more than 5% of all sequencing reads. Identified variants were further filtered based on their presence in repositories of common variations (1000 Genomes, NHLBI exome variant server, and 2,577 noncancer exomes sequenced at Yale). For analysis of the PDXs, we used Xenome to classify the sequence reads and filter out the mouse sequence reads prior to alignment (46).

Cell Lines and PDXs

The UNSCC680AJ cell line utilized in these studies was obtained in 2016 and authenticated via Sanger sequencing for a known alteration in *Kras* (an A59T mutation). The cell line was also tested for *Mycoplasma* and murine viral contamination by the Yale University Molecular Diagnostics Laboratory prior to the experiments reported here. PDX tumors were authenticated by comparative analysis of WES data of the PDX tumor tissue to the patient's tumor tissue at the same stage of disease. The PDXs used in this study maintained 96% (median) of the somatic single nucleotide variants observed in the corresponding patient tumor tissue. All PDXs were housed under guidelines approved by the Yale University Institutional Animal Care and Use Committee (IACUC).

Copy-Number Analysis

Copy-number analysis was performed on WES data using EXCAVATOR software. Briefly, GC content, mappability, and exon size were calculated from the exome and used for exon mean read count data normalization. The hidden Markov model based algorithm was used to determine the boundary of each CNV and each segmented region was called into five copy-number states (homozygous deletion, heterozygous deletion, normal copy number, homozygous copy gain, or multiple copy gain) using the FastCall procedure, which is an algorithm based on a mixture model.

Targeted copy-number analysis was performed for hit validation with TaqMan copy-number assays. For these studies, genomic DNA from tumors or PDXs was extracted using the DNeasy Blood and Tissue Kit (Qiagen #69504). Quantitative PCR was performed with TaqMan copy-number assays (Thermo Fisher Scientific) using a ViiA7 Real-Time PCR System (Thermo Fisher Scientific). Briefly, 10 ng of genomic DNA was used in each reaction. Amplification was carried out for 40 cycles (10 minutes at 95°C, 15 seconds at 95°C, 60 seconds at 60°C). Triplicate CT values were averaged and normalized to genomic DNA from normal tonsil. The TaqMan copy-number reference assay human RNaseP was used for all the reactions. Copy number was evaluated as an average and calculated as $2*2^{-((\text{B2M Ct-RNaseP Ct from PDX})-(\text{B2M Ct-RNaseP Ct from tonsil}))}$. *B2M* copy number was evaluated using two independent assays—Hs00112422_cn and Hs03900880_cn—and the data presented are representative of the average of these two assays ± the standard error of the mean.

Whole-Transcriptome Sequencing

RNA was isolated using RNeasy FFPE kit (Qiagen, #73504). Total RNAs were sequenced on the Illumina HiSeq2500 generating a mean of 57.3 million 76-bp pair-end reads. The low quality base (base quality score < 20) in the last position of the reads was trimmed. The high-quality sequencing reads were aligned to the reference human genome sequence build, hg19, using TopHat v2.1.1, and the raw number of reads mapped on to each gene was counted by HTSeq 0.6 (47, 48). The counts were normalized based on the library size by DESeq2 (49), and differential expression between pre-immunotherapy and immunotherapy-resistant samples was tested by use of the negative binomial distribution.

Immunoblotting

Flash-frozen xenograft tissue was crushed and lysed in RIPA buffer (50 mmol/L Tris [pH 8], 150 mmol/L NaCl, 5 mmol/L MgCl, 1% Triton X-100, 0.5% sodium deoxycholate, 0.1% SDS) supplemented with a protease and phosphatase inhibitor cocktail (Thermo Scientific #78440). Clarified lysates were subjected to SDS-PAGE and transferred onto nitrocellulose membranes. Membranes were blocked for 30 minutes in 5% nonfat dry milk in TBS-T buffer followed by incubation with the following antibodies: human B2M (Cell Signaling Technology, #12851, 1:1,000), mouse B2M (Abcam, ab75853, 1:1,000), phosphorylated STAT1 (Cell Signaling Technology, #14994, 1:1,000), and β-actin (Santa Cruz Biotechnology, sc-47778, 1:2,000). A horseradish peroxidase–conjugated anti-rabbit secondary was used (Cell Signaling Technology, #7074, 1:2,000). Signal detection was achieved using SuperSignal West Pico chemiluminescent substrate (Pierce Biotechnology).

Flow Cytometry

PDXs generated from biopsy specimens were mechanically dissociated by Miltenyi GentleMACS in RPMI + 10% human serum and passed through a 70-μm nylon mesh to create single-cell suspensions. Cells were stained with anti-human B2M (Clone 2M2, BioLegend) and anti-HLA Class I (Clone W6/32, BioLegend) for 30 minutes on ice. As a staining control for B2M and HLA I, a B lymphoblast cell line deficient in B2M (Daudi cells) was stained and analyzed in parallel. In addition, Daudi cells with overexpressed B2M were used as positive controls for B2M and HLA I staining.

Immunohistochemistry

The blocks of FFPE tissue were cut into 4-μm sections. After antigen retrieval, the sections were stained with either a mouse anti–PD-L1 monoclonal antibody (Dako, clone 22C3) or an anti-CD8 antibody (Dako, Clone 144B) with appropriate positive and negative controls.

Syngeneic Tumor Model

The murine lung cancer cell line UNSCC680AJ was cultured in RPMI-1640 medium + L-glutamine (Corning), supplemented with 10% heat-inactivated bovine serum (Atlanta Biologicals) and 1% penicillin/streptomycin (Corning), and was routinely tested for *Mycoplasma*.

A polyclonal B2M knockout UNSCC680AJ cell line was generated by transfection of the PX459 v2.0 plasmid (#62988; Addgene) containing Cas9- and *B2m*-specific sgRNA: 5′-AGTATACTCACGCCAC CCAC-3′. The B2M polyclonal knockout cell line was selected for 2 days in 0.7 μg/mL of puromycin containing complete RPMI media. After 2 days of selection, cells were single-cell sorted using a flow cytometer, and resulting clones were screened for B2M deficiency via Western blotting.

A/J wild-type mice (age, 3–6 weeks) were purchased from The Jackson Laboratory (Stock #000646). All animals were kept in pathogen-free housing under guidelines approved by the Yale University IACUC. Briefly, 5×10^5 UNSCC680AJ cells were subcutaneously injected into the right flank of A/J mice. Antibody treatment started when the tumor volume reached approximately 30 mm^3. Anti–PD-1 (RMP1-14, BioXCell) was injected intraperitoneally at a dose of 100 μg every 3 days for a total of five injections. Isotype-matched IgG (2A3, BioXCell) was administered as a control. The tumor volume was measured every 3 days and was calculated using the following formula: volume = length × $width^2 \times 0.52$.

Cytotoxicity Assay

UNSCC680AJ empty-vector tumors were dissected from the mice and CD8 T cells were isolated from the tumors and spleens using the EasySep Mouse $CD8^+$ T Cell Isolation Kit (STEMCELL Technologies). UNSCC680AJ empty-vector or B2M knockout cell lines were then cocultured *in vitro* with the UNSCC680AJ empty-vector tumor-infiltrating (or spleen) CD8 T cells for 24 hours at the effector/target (E/T) ratios of 0:1, 1:2, and 1:1. Cells were subsequently stained with anti–CD45-Pacific Blue (BioLegend), anti–CD3-APC-eFluor 780 (eBioscience), and anti–CD8-PE (BioLegend) at 4°C for 30 minutes. The cells were then washed, stained with a 7-AAD staining solution (BD Biosciences) for 30 minutes at 4°C, and analyzed by flow cytometry. Target cell killing by tumor-specific CD8 T cells was determined using the following formula adapted from previous reports (50, 51): Percentage of adjusted tumor cell death = (%7AAD$^+$ $CD45^-$ cells with effector T cells − %7AAD$^+$ $CD45^-$ cells without effector T cells). Spontaneous cell death was lower than 6% in all experiments.

Data Archived

Data have been archived at https://www.ncbi.nlm.nih.gov/gap and can be accessed under the study accession number phs001464.v1.p1.

Disclosure of Potential Conflicts of Interest

S. Gettinger is a consultant/advisory board member for BMS, ARIAD, and Pfizer. S.B. Goldberg is a consultant/advisory board member for AstraZeneca. I. Melero reports receiving commercial research grants from Alligator, BMS, and Roche and is a consultant/advisory board member for BMS, Roche, Alligator, Bayer, Lilly, Novartis, and AstraZeneca. D.L. Rimm is a consultant/advisory board member for Perkin Elmer, BMS, AstraZeneca, Cell Signaling Technology, and Merck. K.A. Schalper reports receiving commercial research grants from Tesaro Inc., Onkaido Therapeutics, Takeda, and Surface Oncology, has received honoraria from the speakers bureaus of Takeda and Merck, and is a consultant/advisory board member for Celgene. K. Politi reports receiving commercial research grants from AstraZeneca and Roche and is a consultant/advisory board member for AstraZeneca, Novartis, and Merck. No potential conflicts of interest were disclosed by the other authors.

Authors' Contributions

Conception and design: S. Gettinger, K. Hastings, A. Truini, V.Y. Du, J. Schlessinger, R. Lifton, P. Kavathas, K. Schalper, R.S. Herbst, K. Politi
Development of methodology: S. Gettinger, K. Hastings, A. Truini, I. Datar, G. Cai, V.Y. Du, I. Melero, J. Agorreta, L.M. Montuenga, R. Lifton, S.M. Kaech, K. Schalper, R.S. Herbst, K. Politi
Acquisition of data (provided animals, acquired and managed patients, provided facilities, etc.): S. Gettinger, K. Hastings, A. Truini, I. Datar, R. Sowell, A. Wurtz, G. Cai, S.B. Goldberg, A. Chiang, M.F. Sanmamed, J. Agorreta, L.M. Montuenga, R. Lifton, S.M. Kaech, K. Schalper, R.S. Herbst, K. Politi
Analysis and interpretation of data (e.g., statistical analysis, biostatistics, computational analysis): S. Gettinger, J. Choi, K. Hastings, A. Truini, I. Datar, R. Sowell, W. Dong, V.Y. Du, A. Chiang, I. Melero, J. Agorreta, D.L. Rimm, S.M. Kaech, K. Schalper, R.S. Herbst, K. Politi
Writing, review, and/or revision of the manuscript: S. Gettinger, K. Hastings, A. Truini, I. Datar, R. Sowell, A. Wurtz, W. Dong, G. Cai, M.A. Melnick, S.B. Goldberg, A. Chiang, M.F. Sanmamed, I. Melero, J. Agorreta, L.M. Montuenga, S. Ferrone, P. Kavathas, D.L. Rimm, S.M. Kaech, K. Schalper, R.S. Herbst, K. Politi
Administrative, technical, or material support (i.e., reporting or organizing data, constructing databases): S. Gettinger, K. Hastings, A. Truini, A. Wurtz, M.A. Melnick, J. Schlessinger, R.S. Herbst, K. Politi
Study supervision: S. Gettinger, J. Schlessinger, R. Lifton, R.S. Herbst, K. Politi

Grant Support

This work was supported by the following NIH/NCI grants: the Yale SPORE in Lung Cancer (P50CA196530) to R.S. Herbst, R01CA195720 to K. Politi and S.M. Kaech, and F32CA210516 to K. Hastings. Additional support came from a Stand Up To Cancer Lung Dream grant, Department of Defense Lung Cancer Research Program Career Development Award #LC150383 to K. Schalper, a Lung Cancer Research Foundation grant to K. Schalper, a fellowship from the Italian Association for Cancer Research (AIRC) to A. Truini, the Leslie H. Warner Fellowship to K. Hastings, The Diane and David Heller Foundation, The Beatrice Klienberg Neuwirth Research Program, and the Melissa Marottoli Hogan Foundation. Yale Cancer Center Shared Resources used in this article were in part supported by NIH/NCI Cancer Center Support Grant P30 CA016359.

The costs of publication of this article were defrayed in part by the payment of page charges. This article must therefore be hereby marked *advertisement* in accordance with 18 U.S.C. Section 1734 solely to indicate this fact.

Received May 30, 2017; revised August 25, 2017; accepted September 29, 2017; published OnlineFirst October 12, 2017.

REFERENCES

1. Khalil DN, Smith EL, Brentjens RJ, Wolchok JD. The future of cancer treatment: immunomodulation, CARs and combination immunotherapy. Nat Rev Clin Oncol 2016;13:273–90.
2. Freeman GJ, Long AJ, Iwai Y, Bourque K, Chernova T, Nishimura H, et al. Engagement of the PD-1 immunoinhibitory receptor by a novel

B7 family member leads to negative regulation of lymphocyte activation. J Exp Med 2000;192:1027–34.
3. Zou W, Wolchok JD, Chen L. PD-L1 (B7-H1) and PD-1 pathway blockade for cancer therapy: mechanisms, response biomarkers, and combinations. Sci Transl Med 2016;8:328rv4.
4. Peggs KS, Quezada SA, Chambers CA, Korman AJ, Allison JP. Blockade of CTLA-4 on both effector and regulatory T cell compartments contributes to the antitumor activity of anti-CTLA-4 antibodies. J Exp Med 2009;206:1717–25.
5. Gettinger SN, Horn L, Gandhi L, Spigel DR, Antonia SJ, Rizvi NA, et al. Overall survival and long-term safety of nivolumab (anti-programmed death 1 antibody, BMS-936558, ONO-4538) in patients with previously treated advanced non-small-cell lung cancer. J Clin Oncol 2015;33:2004–12.
6. Borghaei H, Paz-Ares L, Horn L, Spigel DR, Steins M, Ready NE, et al. Nivolumab versus docetaxel in advanced nonsquamous non-small-cell lung cancer. N Eng J Med 2015;373:1627–39.
7. Garon EB, Rizvi NA, Hui R, Leighl N, Balmanoukian AS, Eder JP, et al. Pembrolizumab for the treatment of non-small-cell lung cancer. N Eng J Med 2015;372:2018–28.
8. Brahmer J, Reckamp KL, Baas P, Crino L, Eberhardt WE, Poddubskaya E, et al. Nivolumab versus docetaxel in advanced squamous-cell non-small-cell lung cancer. N Eng J Med 2015;373:123–35.
9. Rittmeyer A, Barlesi F, Waterkamp D, Park K, Ciardiello F, von Pawel J, et al. Atezolizumab versus docetaxel in patients with previously treated non-small-cell lung cancer (OAK): a phase 3, open-label, multicentre randomised controlled trial. Lancet 2017;389:255–65.
10. Reck M, Rodriguez-Abreu D, Robinson AG, Hui R, Csoszi T, Fulop A, et al. Pembrolizumab versus chemotherapy for PD-L1-positive non-small-cell lung cancer. N Eng J Med 2016. DOI: 10.1056/NEJMoa1606774.
11. Herbst RS, Baas P, Kim DW, Felip E, Perez-Gracia JL, Han JY, et al. Pembrolizumab versus docetaxel for previously treated, PD-L1-positive, advanced non-small-cell lung cancer (KEYNOTE-010): a randomised controlled trial. Lancet 2016;387:1540–50.
12. Barlesi F, Steins M, Horn L, Ready N, Felip E, Borghaei H, et al. Long-term outcomes with nivolumab (Nivo) vs docetaxel (Doc) in patients (Pts) with advanced (Adv) NSCLC: CheckMate 017 and CheckMate 057 2-y update. Ann Oncol 2016;27:1215PD.
13. Brahmer J, Horn L, Jackman D, Spigel D, Antonia S, Hellmann M, et al. Five-year follow-up from the CA209-003 study of nivolumab in previously treated advanced non-small cell lung cancer: clinical characteristics of long-term survivors. AACR Annual Meeting Abstract 2017;CT077.
14. Lynch TJ, Bondarenko I, Luft A, Serwatowski P, Barlesi F, Chacko R, et al. Ipilimumab in combination with paclitaxel and carboplatin as first-line treatment in stage IIIB/IV non-small-cell lung cancer: results from a randomized, double-blind, multicenter phase II study. J Clin Oncol 2012;30:2046–54.
15. Zatloukal P, Heo DS, Park K, Kang J, Butts C, Bradford D, et al. Randomized phase II clinical trial comparing tremelimumab (CP-675,206) with best supportive care (BSC) following first-line platinum-based therapy in patients (pts) with advanced non-small cell lung cancer (NSCLC). J Clin Oncol 2009;27:abstr 8071.
16. Hellmann MD, Rizvi NA, Goldman JW, Gettinger SN, Borghaei H, Brahmer JR, et al. Nivolumab plus ipilimumab as first-line treatment for advanced non-small-cell lung cancer (CheckMate 012): results of an open-label, phase 1, multicohort study. Lancet Oncol 2017;18:31–41.
17. Antonia S, Goldberg SB, Balmanoukian A, Chaft JE, Sanborn RE, Gupta A, et al. Safety and antitumour activity of durvalumab plus tremelimumab in non-small cell lung cancer: a multicentre, phase 1b study. Lancet Oncol 2016;17:299–308.
18. Rizvi NA, Hellmann MD, Snyder A, Kvistborg P, Makarov V, Havel JJ, et al. Mutational landscape determines sensitivity to PD-1 blockade in non-small cell lung cancer. Science (New York, NY 2015;348:124–8.
19. Snyder A, Makarov V, Merghoub T, Yuan J, Zaretsky JM, Desrichard A, et al. Genetic basis for clinical response to CTLA-4 blockade in melanoma. N Eng J Med 2014;371:2189–99.
20. Van Allen EM, Miao D, Schilling B, Shukla SA, Blank C, Zimmer L, et al. Genomic correlates of response to CTLA-4 blockade in metastatic melanoma. Science (New York, NY 2015;350:207–11.
21. Anagnostou V, Smith KN, Forde PM, Niknafs N, Bhattacharya R, White J, et al. Evolution of neoantigen landscape during immune checkpoint blockade in non-small cell lung cancer. Cancer Discov 2017;7:264–76.
22. Zaretsky JM, Garcia-Diaz A, Shin DS, Escuin-Ordinas H, Hugo W, Hu-Lieskovan S, et al. Mutations associated with acquired resistance to PD-1 blockade in melanoma. N Eng J Med 2016;375:819–29.
23. Shin DS, Zaretsky JM, Escuin-Ordinas H, Garcia-Diaz A, Hu-Lieskovan S, Kalbasi A, et al. Primary resistance to PD-1 blockade mediated by JAK1/2 mutations. Cancer Discov 2017;7:188–201.
24. Le DT, Durham JN, Smith KN, Wang H, Bartlett BR, Aulakh LK, et al. Mismatch repair deficiency predicts response of solid tumors to PD-1 blockade. Science 2017;357:409–13.
25. Campbell JD, Alexandrov A, Kim J, Wala J, Berger AH, Pedamallu CS, et al. Distinct patterns of somatic genome alterations in lung adenocarcinomas and squamous cell carcinomas. Nat Genet 2016;48:607–16.
26. Alexandrov LB, Nik-Zainal S, Wedge DC, Aparicio SA, Behjati S, Biankin AV, et al. Signatures of mutational processes in human cancer. Nature 2013;500:415–21.
27. Alexandrov LB, Ju YS, Haase K, Van Loo P, Martincorena I, Nik-Zainal S, et al. Mutational signatures associated with tobacco smoking in human cancer. Science 2016;354:618–22.
28. Tran E, Robbins PF, Lu YC, Prickett TD, Gartner JJ, Jia L, et al. T-cell transfer therapy targeting mutant KRAS in cancer. N Eng J Med 2016;375:2255–62.
29. Restifo NP, Marincola FM, Kawakami Y, Taubenberger J, Yannelli JR, Rosenberg SA. Loss of functional beta 2-microglobulin in metastatic melanomas from five patients receiving immunotherapy. J Nat Cancer Inst 1996;88:100–8.
30. D'Urso CM, Wang ZG, Cao Y, Tatake R, Zeff RA, Ferrone S. Lack of HLA class I antigen expression by cultured melanoma cells FO-1 due to a defect in B2m gene expression. J Clin Invest 1991;87:284–92.
31. Azpilikueta A, Agorreta J, Labiano S, Perez-Gracia JL, Sanchez-Paulete AR, Aznar MA, et al. Successful immunotherapy against a transplantable mouse squamous lung carcinoma with anti-PD-1 and anti-CD137 monoclonal antibodies. J Thorac Oncol 2016;11:524–36.
32. Kelderman S, Schumacher TN, Haanen JB. Acquired and intrinsic resistance in cancer immunotherapy. Mol Oncol 2014;8:1132–9.
33. Gao J, Shi LZ, Zhao H, Chen J, Xiong L, He Q, et al. Loss of IFN-gamma pathway genes in tumor cells as a mechanism of resistance to anti-CTLA-4 therapy. Cell 2016;167:397–404 e9.
34. del Campo AB, Kyte JA, Carretero J, Zinchencko S, Mendez R, Gonzalez-Aseguinolaza G, et al. Immune escape of cancer cells with beta2-microglobulin loss over the course of metastatic melanoma. Int J Cancer 2014;134:102–13.
35. Sucker A, Zhao F, Real B, Heeke C, Bielefeld N, Mabetaen S, et al. Genetic evolution of T-cell resistance in the course of melanoma progression. Clin Cancer Res 2014;20:6593–604.
36. Paschen A, Arens N, Sucker A, Greulich-Bode KM, Fonsatti E, Gloghini A, et al. The coincidence of chromosome 15 aberrations and beta2-microglobulin gene mutations is causative for the total loss of human leukocyte antigen class I expression in melanoma. Clin Cancer Res 2006;12:3297–305.
37. Campoli M, Ferrone S. HLA antigen changes in malignant cells: epigenetic mechanisms and biologic significance. Oncogene 2008;27:5869–85.
38. Chang CC, Campoli M, Ferrone S. Classical and nonclassical HLA class I antigen and NK Cell-activating ligand changes in malignant cells: current challenges and future directions. Adv Cancer Res 2005;93:189–234.
39. Bernal M, Ruiz-Cabello F, Concha A, Paschen A, Garrido F. Implication of the beta2-microglobulin gene in the generation of tumor escape phenotypes. Cancer Immunol Immunother 2012;61:1359–71.
40. Benitez R, Godelaine D, Lopez-Nevot MA, Brasseur F, Jimenez P, Marchand M, et al. Mutations of the beta2-microglobulin gene result

in a lack of HLA class I molecules on melanoma cells of two patients immunized with MAGE peptides. Tissue Antigens 1998;52:520–9.
41. Scuoppo C, Miething C, Lindqvist L, Reyes J, Ruse C, Appelmann I, et al. A tumour suppressor network relying on the polyamine-hypusine axis. Nature 2012;487:244–8.
42. Cai Y, Crowther J, Pastor T, Abbasi Asbagh L, Baietti MF, De Troyer M, et al. Loss of chromosome 8p governs tumor progression and drug response by altering lipid metabolism. Cancer Cell 2016; 29:751–66.
43. Pereira C, Gimenez-Xavier P, Pros E, Pajares MJ, Moro M, Gomez A, et al. Genomic profiling of patient-derived xenografts for lung cancer identifies B2M inactivation impairing immunorecognition. Clin Cancer Res 2017. doi: 10.1158/1078-0432
44. Kleffel S, Posch C, Barthel SR, Mueller H, Schlapbach C, Guenova E, et al. Melanoma cell-intrinsic PD-1 receptor functions promote tumor growth. Cell 2015;162:1242–56.
45. Koyama S, Akbay EA, Li YY, Herter-Sprie GS, Buczkowski KA, Richards WG, et al. Adaptive resistance to therapeutic PD-1 blockade is associated with upregulation of alternative immune checkpoints. Nat Commun 2016;7:10501.
46. Conway T, Wazny J, Bromage A, Tymms M, Sooraj D, Williams ED, et al. Xenome–a tool for classifying reads from xenograft samples. Bioinformatics 2012;28:i172–8.
47. Kim D, Pertea G, Trapnell C, Pimentel H, Kelley R, Salzberg SL. TopHat2: accurate alignment of transcriptomes in the presence of insertions, deletions and gene fusions. Genome Biol 2013;14:R36.
48. Anders S, Pyl PT, Huber W. HTSeq–a Python framework to work with high-throughput sequencing data. Bioinformatics 2015;31:166–9.
49. Love MI, Huber W, Anders S. Moderated estimation of fold change and dispersion for RNA-seq data with DESeq2. Genome Biol 2014;15:550.
50. Loffredo JT, Burwitz BJ, Rakasz EG, Spencer SP, Stephany JJ, Vela JP, et al. The antiviral efficacy of simian immunodeficiency virus-specific CD8+ T cells is unrelated to epitope specificity and is abrogated by viral escape. J Virol 2007;81:2624–34.
51. Carlson JM, Du VY, Pfeifer N, Bansal A, Tan VY, Power K, et al. Impact of pre-adapted HIV transmission. Nat Med 2016;22:606–13.